buildings

MDPI

*Article*

# Mechanical Properties of S235 Steel Protected with Intumescent Coatings Under High Temperatures: An Experimental Study

**Casim Yazici**

Department of Construction, Ağrı İbrahim Çeçen University, 04400 Agri, Turkey; cyazici@agri.edu.tr

**Abstract:** This study investigates the impact of high temperatures on the mechanical properties of fire-protected versus unprotected S235 cold-formed steel (CFS) specimens with variable thicknesses. Through axial tensile tests, we assessed how intumescent coatings influence the behavior of steel under fire-like conditions. The results reveal that as temperatures increase, the mechanical strength of unprotected steel diminishes significantly, especially at temperatures beyond 400 °C. However, at temperatures between 500 and 900 °C, coated specimens demonstrate considerably enhanced strength compared to their uncoated counterparts. The coating effectively reduces the steel's temperature exposure by approximately 200 °C, crucially preserving its integrity at critical temperatures. The thickness of the steel also plays a role, with thicker specimens maintaining higher ultimate strength up to a threshold temperature. The study culminates in a predictive analytical model that estimates the ultimate strength of coated and uncoated steel based on temperature and specimen thickness. These insights contribute substantially to the design of safer, more fire-resistant steel structures.

**Keywords:** rising temperature periods; cold-formed steel; steel; maximum temperature influence coefficient; temperature history; fire protection; intumescent coatings



**Citation:** Yazici, C. Mechanical Properties of S235 Steel Protected with Intumescent Coatings Under High Temperatures: An Experimental Study. *Buildings* **2024**, *14*, 1597. https://doi.org/10.3390/buildings14061597

Academic Editors: Xiaoming Liu and Jianguo Jiang

Received: 25 March 2024
Revised: 5 May 2024
Accepted: 8 May 2024
Published: 31 May 2024



## 1. Introduction

Recent trends in construction demand robust fire safety measures, especially in relation to the behavior of steel under high temperatures, which has led to an increase in incidents of catastrophic fires in urban settings. Despite the advances in fire-resistant materials, significant vulnerabilities still exist, particularly with cold-formed thin-walled steel profiles. These profiles, which are commonly used due to their cost-effectiveness and ease of installation, are less resistant to fire compared to their hot-rolled counterparts, a fact that has been well documented in various studies [1–9]. For instance, research has shown that a marked decrease in mechanical strength and stiffness occurs as temperatures rise, with critical degradation occurring between 550 and 600 °C [10–15].

Active and passive fire protection measures are crucial in mitigating these weaknesses. Among passive measures, intumescent coatings are particularly valued for their ability to significantly delay structural steel from reaching critical temperatures [16–20]. This study aims to build on the foundational work on this topic by exploring how different thicknesses of intumescent coatings influence the thermal and mechanical performance of steel under varied high-temperature scenarios.

The specific objectives of this study are to:

Quantitatively assess the effectiveness of intumescent coatings in improving the fire resistance of cold-formed steel.

Determine the impact of varying thicknesses of steel and coatings on the structural integrity during and after exposure to high temperatures.

Develop a predictive model that estimates the ultimate strength of coated and uncoated steel based on empirical data, providing a practical tool for structural engineers.

By addressing these goals, this research seeks to fill a gap in the current understanding of fire-resistant technologies, particularly regarding how intumescent coatings can be optimized to enhance the safety and durability of steel structures exposed to fire.

Mass manufacturing and simple installation are made possible by cold-formed thin-walled steel profiles made using cold-shaping techniques [21]. Storage rack system members which are produced by the cold-forming method have open sections with indentations, projections, and gaps. Steel constructions and storage rack systems are becoming subject to increased demand as a result of the current surge in distant sales techniques. Along with this increasing demand, the heights of storage rack systems are also on the rise [22]. After the fire incident at the American World Trade Center on September 11th, academics and structural engineers turned their attention to examining the behavior of steel during and after fires. They have carried out numerous studies to explore the behavior of steel exposed to fire [1–9]. Cold-formed steel profiles are less fire-resistant than hot-rolled profiles. Fire resistance depends on the section factor, which is derived based on the relationship between the surface area exposed to fire and the volume of steel [10]. Experimental and finite element analyses have been conducted to investigate the low fire resistance of cold-formed steel profiles [11–15].

This study investigates the thermal protective properties of inorganic intumescent coatings applied to steel structures, focusing on the mechanisms of heat transfer during exposure to fire. Using cone calorimeter testing, Kang, Choi, and Choi examine the expansion process of the coatings, which form a porous, char-like layer that acts as a thermal barrier. The research highlights how the porosity and thermal conductivity of the expanded material are critical in enhancing its effectiveness at insulating the substrate against high temperatures. By providing a detailed analysis of these properties, the study significantly contributes to the understanding of fire-retardant materials' functionality, offering valuable insights for improving fire safety in modern building design [23].

Under normal circumstances, steel structural elements exhibit extremely effective strength and stiffness; however, they rapidly lose these features at rising temperatures due to the increase in ambient temperature [24]. Despite having a high heat conductivity, steel is essentially non-combustible. But the amount of stress that steel can withstand during a fire or at high temperatures can have a big impact on how much load it can support. Depending on the carbon content in the steel, critical temperatures are generally considered to be between 550 and 600 °C. In addition, the yield strength of steel is reduced by more than 50% compared to its strength at room temperature [21]. This decrease in strength occurs along with a reduction in the ductility of the element [24]. Light steel systems also exhibit significant vulnerability in terms of fire behavior due to the structural nature of steel. As a result, structural fire designs need to include certain measures. The primary goal of fire safety measures is to keep people safe while minimizing material damage. These measures can be grouped into two major categories: active and passive protection [25]. Active protection systems, also referred to as active systems, are fire safety precautions in buildings that help put out fires, let occupants escape, and stop or slow the spread of a fire. They can be categorized into two main sections: fire detection and warning systems (detectors and alarm buttons) and fire prevention and suppression systems (sprinklers). Materials for passive protection can be divided into two primary groups: reactive and non-reactive. When exposed to high temperatures during a fire, non-reactive protection products retain their qualities; the most frequently employed products are coatings and sprays. Reactive protection materials, however, are materials whose properties change along with the fire conditions. Among these, expanding (intumescent) coatings are widely used and preferred [16–20]. Intumescent coats expand and swell when exposed to heat and flames during a fire, forming a thick foam-like layer similar to charcoal. This foam layer acts as a barrier that prevents the surface from coming into contact with air, heat, and fire, thus delaying ignition or slowing down the spread of fire within the applied material. These coats are applied to steel surfaces to provide fire protection. Depending on the amount of heat generated during a fire, intumescent coats can expand to 2–100 times

their original applied thickness, and they typically provide 30–120 min of fire resistance. Intumescent coats, while similar in appearance to traditionally used coats, are categorized into two types: water- or solvent-based (mixable with water and used as a solvent) and epoxy-based (mastics or thick film coatings). Intumescent coats are administrated in three layers: a protective primer layer that protects against rust, an expanding composition layer, and a decorative layer. These expanding coats are favored in steel structures, especially due to their architectural and aesthetic significance. They are also preferred because they can be applied more quickly and easily on complex surfaces compared to other passive fire protection materials [23,26–38].

Actual developments in numerical simulations of the structural behavior in fire situation are focusing on taking into consideration the interaction of all structural members in a global approach. Therefore, it is necessary to simulate the load-bearing behavior of connections. With this motivation, the authors conducted experiments and thermal FE-simulations on two different connection types. In this paper, the accompanying mechanical FE-simulations of both investigated connection types will be described. The joints are defined as an end plate connection in a steel structure and a fin plate connection in a composite structure. In addition to validating the numerical models, the results of the described investigations show that it is possible to activate a significant moment of resistance within fin plate connections of composite structures. The main requirement for this activation is sufficient reinforcement strength [39,40]. The study includes experimental investigations on coated beams and columns connected to space-enclosing elements and numerical simulations for temperature field calculations, incorporating the expansion process of the intumescent coating [41].

One of the most significant reasons for the limited use of fire-retardant coats is their expensive nature. Yet, even using active protection measures like sprinklers may not provide complete protection against the effects of a fire. This is due to the possibility that, in the event of a fire, water from ceiling-level sprinklers may not reach the lower-level shelves, and this will not contribute effectively to extinguishing the fire. In the context of potential fire situations in storage rack systems, a noteworthy study was conducted by Ren et al. (2020). In this study, attention was drawn to this issue, and the structural behavior of the lower-level elements of the rack system was investigated by applying fire effects [42].

During a fire, intumescent fire-resistant coatings expand to several times their original applied thickness, creating a thermal barrier between the fire and the structural steel. These coatings swell and form an insulating char layer, acting as a thin fire-resistant coating. This prevents the steel elements from reaching critical temperatures during a fire, thereby assisting in maintaining the structural integrity of the building [8]. Due to their aesthetic appearance, versatility, quick application, and ease of inspection and maintenance, passive fire protection for load-bearing steel frame structures is preferred by architects and designers. This study conducted axial tensile tests on S235 cold-formed steel samples subjected to increasing temperature periods. This study examined the mechanical behavior of coated and uncoated samples at different temperatures, utilizing elastic modulus, yield strength/strain, and ultimate strength/strain values. The research provides comparative results of the mechanical properties of coated and uncoated samples at elevated temperature levels during a fire event. This article investigates the use of passive fire protection, specifically intumescent coatings, on cold-formed steel in the literature. It explores how these coatings can preserve structural properties after exposure to high temperatures in storage rack systems. Considering this context, the study examines the loss of mechanical properties after high-temperature effects on coated and uncoated tensile specimens.

## 2. Experimental Set-Up

### *2.1. Test Set-Up and Procedure*

In the experiments, a Thermcore PLF 130/25 brand furnace shown in Figure 1a was employed to apply high-temperature effects to the specimens. The mechanical characteristics of the tensile coupons were determined using the Besmak Servo Hydraulic Universal

Test machine depicted in Figure 1b. A type K thermocouple was placed to obtain the temperature inside the furnace and the furnace curve.

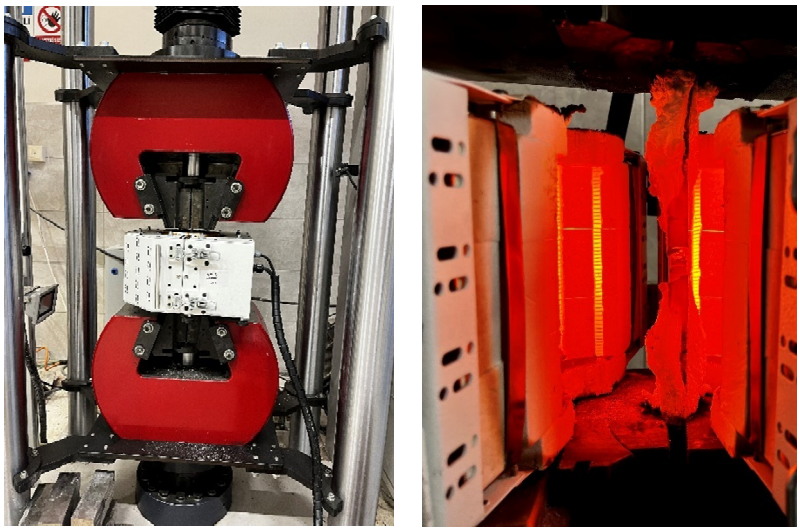

(**a**) (**b**)

**Figure 1.** (**a**) Hydraulic universal test machine. (**b**) High-temperature furnace.

The samples underwent axial tension testing after reaching the target temperature and were maintained at that temperature for 20 min. The furnace heating rate was set to 20 °C/min. The furnace curve was incrementally raised from 23 °C to 1100 °C in increments of 100 °C, and the dwell time at the target temperature is presented in Figure 2. Following this, a steady-state tensile test was conducted, during which the temperature of the specimen was kept constant and the displacement rate was controlled at 0.3 mm/min [43].

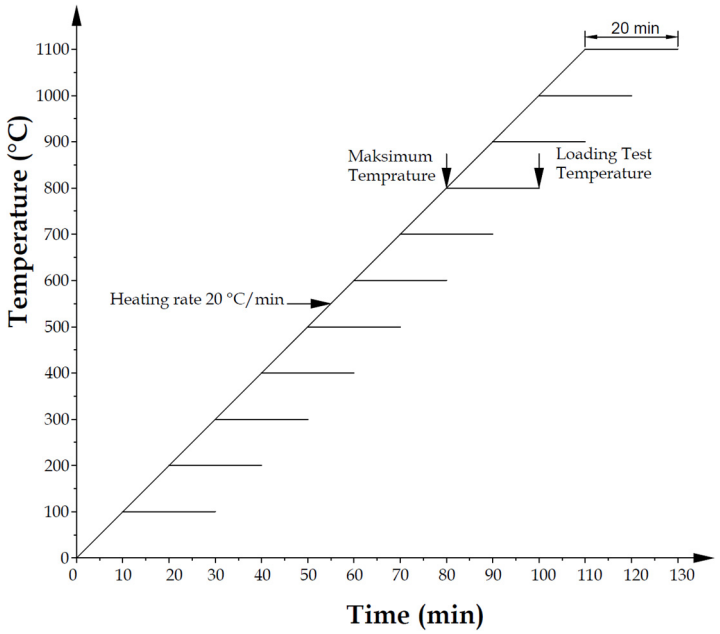


**Figure 2.** High-temperature furnace heating curves.

### *2.2. Test Specimens*

The tensile test specimens were prepared from S235 cold-formed steel (CFS) with thicknesses of 4, 6, 8, 10, and 12 mm (Figure 3). The samples were categorized into two groups: protected and unprotected. All surfaces of the protected test specimens received a gradual application of a water-based fire-retardant coat, which was approximately

250 microns thick. After the coating process, the coat thickness was checked using a coat thickness measurement device. For each thickness, a total of 115 tensile tests were conducted, including both coated and uncoated specimens, starting from 23 °C and increasing in 100 °C increments up to a maximum of 1100 °C.

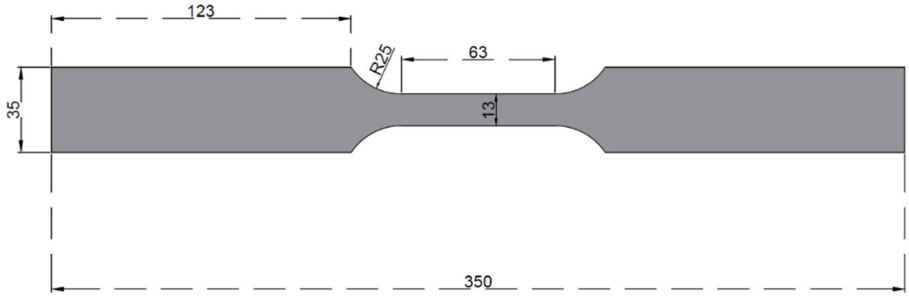


**Figure 3.** The dimensions of the test specimens (units in mm).

On all surfaces of the test specimens, an approximate 250 μm thickness water-based intumescent fire-resistant coat was applied. The coating's chemical components include ammonium polyphosphate (about 28%) as an acid source, pentaerythritol (around 10%) as a carbon source, and melamine (10%) as an expansion agent. Water, cellulose thickener, foam suppressant, biocide, binder, acrylic copolymer emulsion, titanium dioxide, and copolymer dispersion are among the other raw materials. After coating, necessary checks were performed using coat thickness measurement devices. A total of 105 test specimens were prepared to perform tension tests with protected and unprotected conditions at target temperature levels. The technical specifications of the fire-resistant coating are presented, in Table 1. In Table 1, we have clarified the fire-retardant properties of the paint used in our study. The flame-retardant indicators for intumescent coatings include char formation, which acts as an insulating barrier that protects the substrate from fire damage [44], and heat release rate (HRR), a key indicator of the flammability of the coating, which we measured using cone calorimeter tests to confirm its flame-retardant nature [44]. Additionally, we assessed the fire propagation index according to the BS 476: Part 6 standard [45], where the paint exhibited a low index, qualifying it as Class 0 material [44]. The fire resistance limit, defined as the duration for which the coating withstands fire exposure before failure, was evaluated using a small-scale fireproof testing furnace, where the coating demonstrated significant fire resistance [46]. The paint exhibited fire resistance for up to 90 min, depending on the coating thickness and volume ratio of the intumescent ingredients, making it suitable for structural steel protection.

**Table 1.** Technical specifications of fire-retardant coat.

| Ingredient | Water-Based |
|---|---|
| Color | White (ral colors) |
| Applied Temperature | +5∼+35 °C |
| Density | 1.20∼1.40 g/cm$^3$ |
| Viscosity | 10,000∼12,000 mPa·s/25 °C |
| Ph | 7.0∼9.0/25 °C |
| Powder Drying | 45∼60 min/25 °C |
| Touch Dry | 3 h/25 °C |
| Complete (Full) Drying | 24 h/25 °C |

To enhance the scientific merit of our study, we included a comparison with other types of fire-retardant paints, referencing studies on different intumescent coatings, such as those incorporating graphene oxide and other flame-retardant additives [46–50]. We also updated the manuscript to provide a detailed description of the intumescent coating, which includes ammonium polyphosphate as an acid source, pentaerythritol as a carbon

source, and melamine as an expansion agent. While it is true that many intumescent materials protect steel, our study aimed to explore the effectiveness of different formulations on the thermal and mechanical performance of steel under varied high-temperature scenarios [44], contributing valuable insights for fire-resistant steel design.

## 3. Test Results and Discussion

### *3.1. Stress–Strain Curves*

The test specimens that reached the target temperatures were subjected to axial tension after being maintained at the target temperature for 20 min. Figure 4 shows the stress–strain curves of uncoated 4 mm thick specimens, Figure 5 depicts the stress–strain curves of coated 4 mm thick specimens, Figure 6 displays the stress–strain curves of uncoated 6 mm thick specimens, Figure 7 illustrates the stress–strain curves of coated 6 mm thick specimens, Figure 8 presents the stress–strain curves of uncoated 8 mm thick specimens, Figure 9 exhibits the stress–strain curves of coated 8 mm thick specimens, Figure 10 portrays the stress–strain curves of uncoated 10 mm thick specimens, Figure 11 represents the stress–strain curves of coated 10 mm thick specimens, Figure 12 outlines the stress–strain curves of uncoated 12 mm thick specimens, and Figure 13 showcases the stress–strain curves of coated 12 mm thick specimens. When examining the stress–strain curves, it can be observed that yield strength and ultimate strength decrease as the target temperature increases. When comparing the mechanical properties of specimens with the same thickness, significant differences are observed between coated and uncoated samples. Furthermore, when comparing the maximum strength capacity, it has been determined that the strength of coated samples is higher than that of uncoated samples. Figure 14 presents the structural changes in the coat and fracture surface images of both coated and uncoated test specimens after the experiment.

### *3.2. Material Properties' Reduction Factors*

The comparison of the test specimens included the mechanical parameters of the elastic modulus, yield strength, and ultimate strength. The yield strength was identified as the lower yield point of the yield region in the stress–strain curve, the ultimate strength was identified as the highest stress value in the stress–strain curve, and the elastic modulus was identified as the slope of the linear portion of the stress–strain curve. In the study, once the samples reached the target temperature, they were held at that temperature for 20 min before the axial tensile test was initiated. To compare the mechanical characteristics of coated and uncoated specimens at different temperatures, the ratios of the mechanical values at the target temperature to the mechanical values at room temperature were provided. The proportional values of elastic modulus, yield strength, and ultimate strength at elevated temperatures were presented with respect to the mechanical values at room temperature. For instance, in the expression $E_a/E_b$, $E_a$ represents the elastic modulus of the specimen at the target temperature and $E_b$ represents the elastic modulus of the specimen at room temperature. The ratio $E_a/E_b$ provides us with a reduction factor value in terms of the elastic modulus. Similar procedures were applied for yield strength and ultimate strength as well. Reduction factor values were calculated for both coated and uncoated specimens, and these values are presented for each thickness in Tables 2–6. The reduction factor values for the ultimate strengths of protected/unprotected specimens with varying thicknesses during the increasing temperature periods are provided in Figures 15–18.

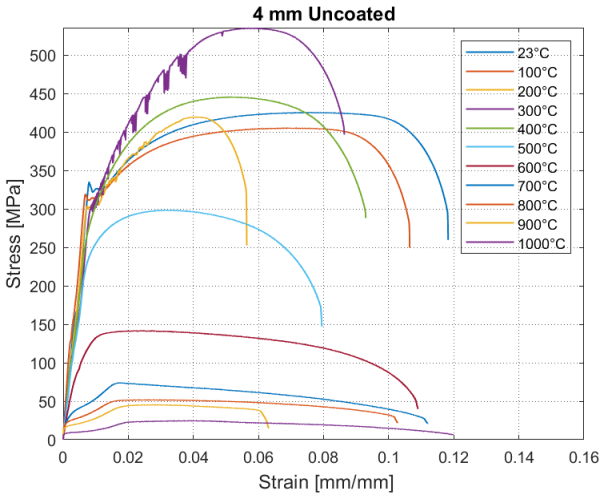


**Figure 4.** Stress–strain curve of uncoated 4 mm specimens.

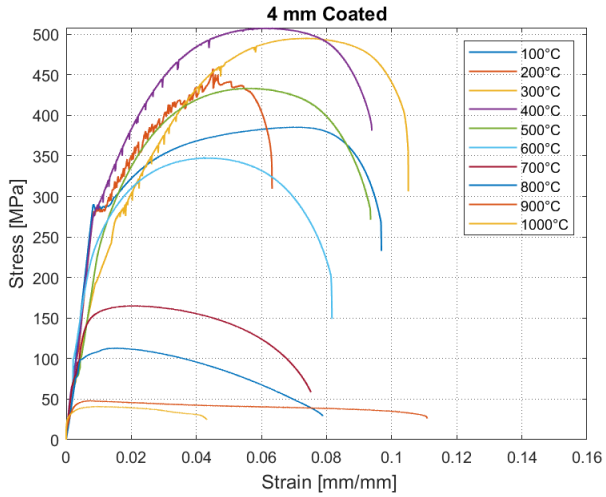


**Figure 5.** Stress–strain curve of 4 mm coated specimens.

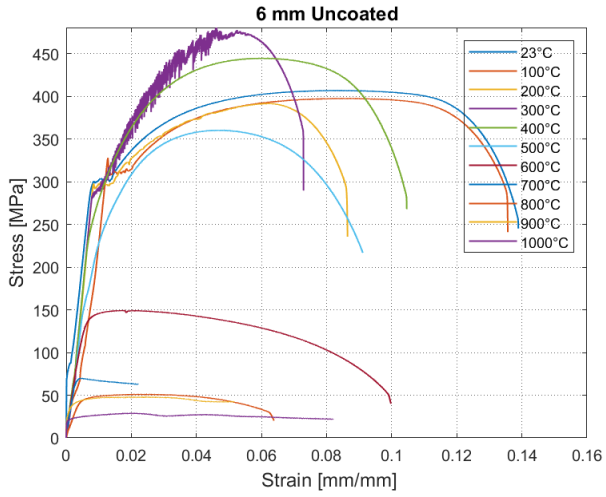


**Figure 6.** Stress–strain curve of 6 mm uncoated specimens.

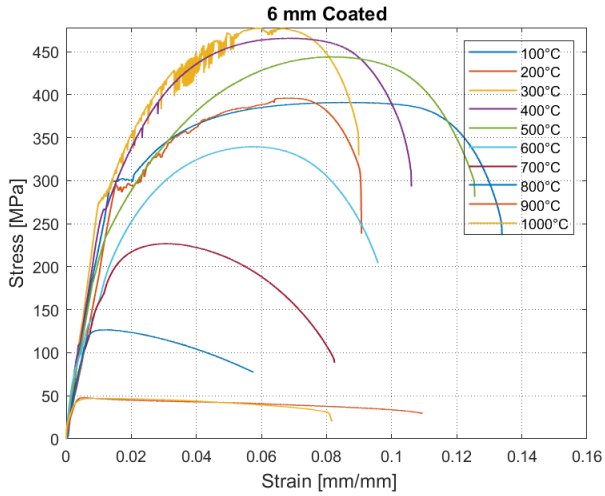


**Figure 7.** Stress–strain curve of 6 mm coated specimens.

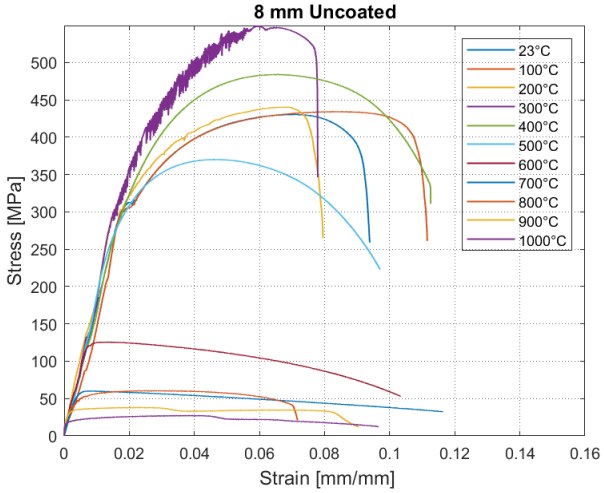


**Figure 8.** Stress–strain curve of 8 mm uncoated specimens.

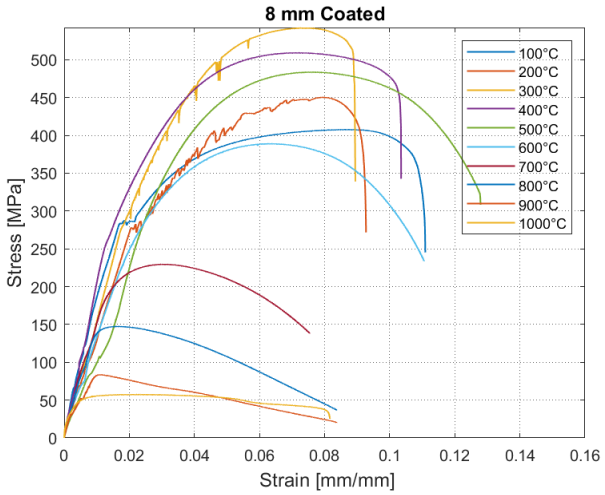


**Figure 9.** Stress–strain curve of 8 mm coated specimens.

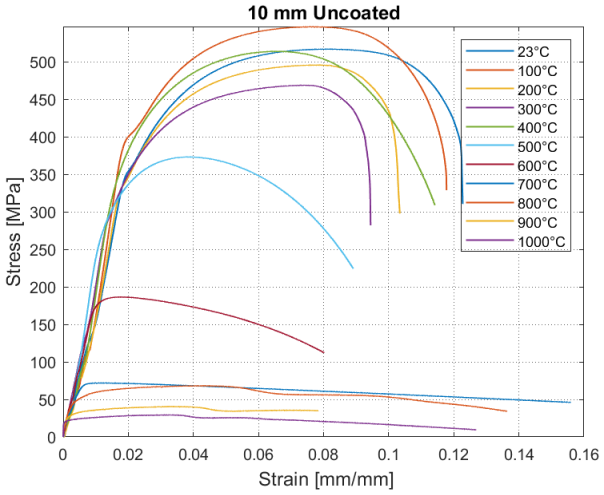


**Figure 10.** Stress–strain curve of 10 mm uncoated specimens.

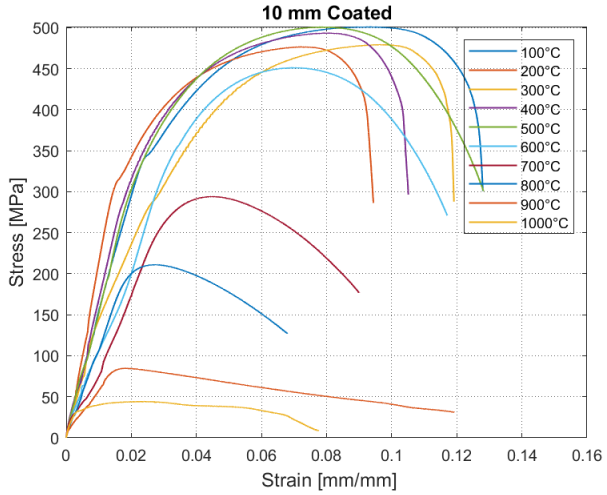


**Figure 11.** Stress–strain curve of 10 mm coated specimens.

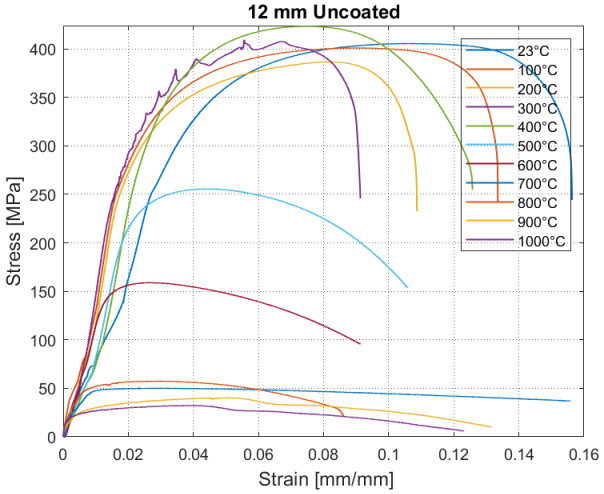


**Figure 12.** Stress–strain curve of 12 mm uncoated specimens.

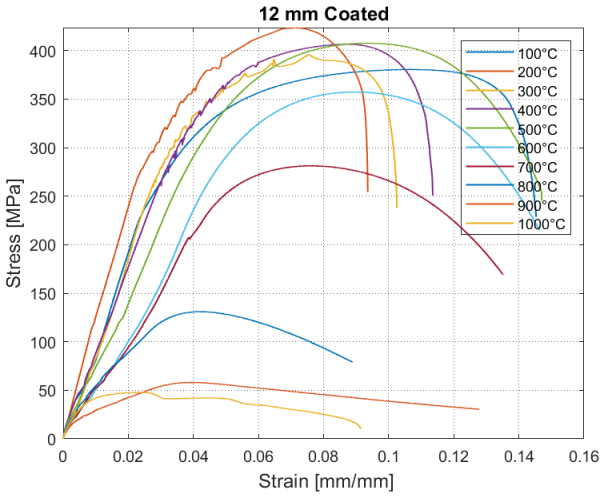


**Figure 13.** Stress–strain curve of 12 mm coated specimens.

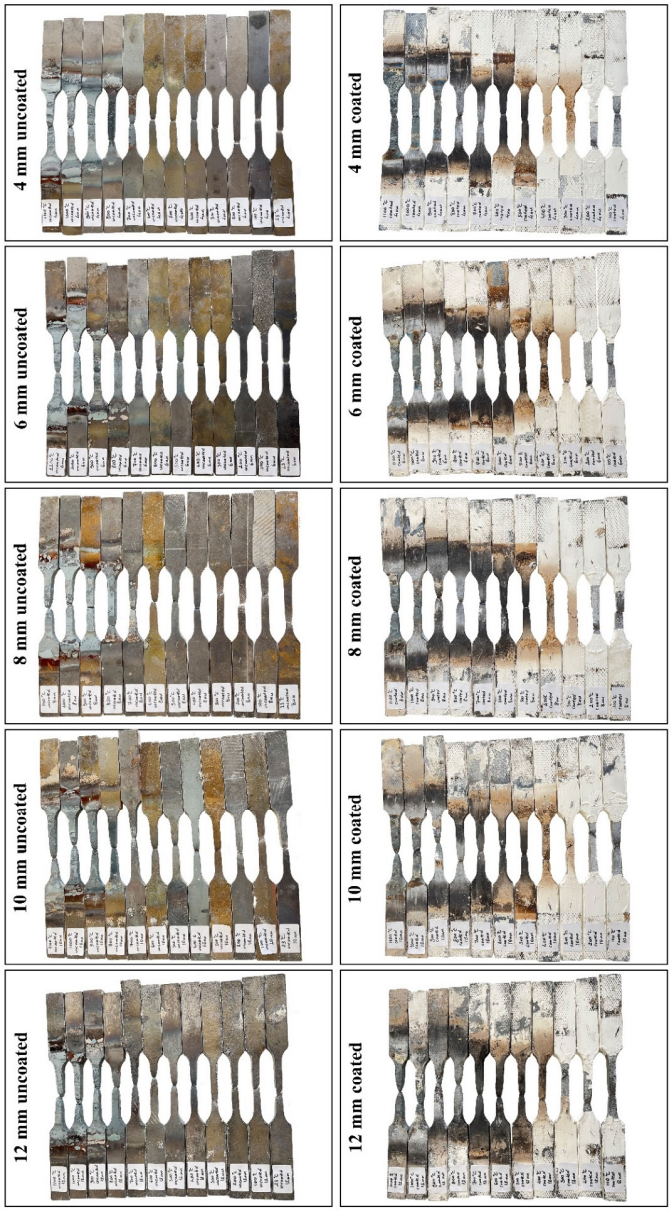


**Figure 14.** Fracture surfaces of the test specimens after exposure to fire.

**Table 2.** Average reduction factor values of S235 4 mm steel at increasing temperatures.

| Maximum Temp. (°C) a | Test Samples Thickness (mm) | Coated | | | Uncoated | | |
|---|---|---|---|---|---|---|---|
| | | $E_a/E_a$ | $F_{a,y}/F_{a,y}$ | $F_{a,u}/F_{a,u}$ | $E_a/E_a$ | $F_{a,y}/F_{a,y}$ | $F_{a,u}/F_{a,u}$ |
| 23 | 4 | | | | 1.000 | 1.000 | 1.000 |
| 100 | | 1.000 | 1.000 | 1.000 | 1.082 | 0.978 | 0.953 |
| 200 | | 0.885 | 0.981 | 1.186 | 1.012 | 0.941 | 0.986 |
| 300 | | 0.598 | 0.691 | 1.284 | 1.001 | 0.926 | 1.258 |
| 400 | | 0.937 | 0.967 | 1.317 | 0.908 | 0.833 | 1.048 |
| 500 | | 0.643 | 0.909 | 1.125 | 0.801 | 0.701 | 0.702 |
| 600 | | 0.953 | 0.625 | 0.903 | 0.383 | 0.377 | 0.334 |
| 700 | | 0.668 | 0.487 | 0.429 | 0.109 | 0.185 | 0.175 |
| 800 | | 0.693 | 0.335 | 0.294 | 0.052 | 0.123 | 0.123 |
| 900 | | 0.379 | 0.145 | 0.125 | 0.030 | 0.105 | 0.107 |
| 1000 | | 0.503 | 0.114 | 0.107 | 0.014 | 0.056 | 0.058 |
| 1100 | | 0.009 | 0.045 | 0.054 | 0.007 | 0.031 | 0.031 |

**Table 3.** Average reduction factor values of S235 6 mm steel at increasing temperatures.

| Maximum Temp. (°C) a | Test Samples Thickness (mm) | Coated | | | Uncoated | | |
|---|---|---|---|---|---|---|---|
| | | $E_a/E_a$ | $F_{a,y}/F_{a,y}$ | $F_{a,u}/F_{a,u}$ | $E_a/E_a$ | $F_{a,y}/F_{a,y}$ | $F_{a,u}/F_{a,u}$ |
| 23 | 6 | | | | 1.000 | 1.000 | 1.000 |
| 100 | | 1.000 | 1.000 | 1.000 | 1.125 | 1.040 | 0.977 |
| 200 | | 0.896 | 0.983 | 1.013 | 1.679 | 1.000 | 0.962 |
| 300 | | 1.230 | 0.934 | 1.221 | 1.748 | 0.950 | 1.180 |
| 400 | | 1.084 | 0.891 | 1.191 | 1.649 | 0.790 | 1.093 |
| 500 | | 1.032 | 0.791 | 1.136 | 1.388 | 0.743 | 0.886 |
| 600 | | 0.916 | 0.669 | 0.869 | 1.173 | 0.400 | 0.367 |
| 700 | | 0.738 | 0.517 | 0.581 | 1.127 | 0.200 | 0.172 |
| 800 | | 0.897 | 0.331 | 0.325 | 0.479 | 0.133 | 0.126 |
| 900 | | 0.685 | 0.136 | 0.123 | 0.702 | 0.117 | 0.118 |
| 1000 | | 0.526 | 0.146 | 0.121 | 0.106 | 0.073 | 0.071 |
| 1100 | | 0.098 | 0.079 | 0.067 | 0.023 | 0.040 | 0.037 |

**Table 4.** Average reduction factor values of S235 8 mm steel at increasing temperatures.

| Maximum Temp. (°C) a | Test Samples Thickness (mm) | Coated | | | Uncoated | | |
|---|---|---|---|---|---|---|---|
| | | $E_a/E_a$ | $F_{a,y}/F_{a,y}$ | $F_{a,u}/F_{a,u}$ | $E_a/E_a$ | $F_{a,y}/F_{a,y}$ | $F_{a,u}/F_{a,u}$ |
| 23 | 8 | | | | 1.000 | 1.000 | 1.000 |
| 100 | | 1.000 | 1.000 | 1.000 | 0.828 | 0.978 | 1.009 |
| 200 | | 0.769 | 0.993 | 1.105 | 1.043 | 0.971 | 1.022 |
| 300 | | 0.906 | 1.014 | 1.330 | 1.046 | 0.942 | 1.275 |
| 400 | | 1.198 | 0.996 | 1.249 | 0.934 | 1.051 | 1.124 |
| 500 | | 0.613 | 1.389 | 1.186 | 1.104 | 0.808 | 0.860 |
| 600 | | 0.751 | 0.842 | 0.954 | 0.952 | 0.378 | 0.292 |
| 700 | | 0.873 | 0.632 | 0.564 | 0.813 | 0.154 | 0.140 |
| 800 | | 0.831 | 0.477 | 0.362 | 0.591 | 0.157 | 0.141 |
| 900 | | 0.462 | 0.246 | 0.206 | 0.560 | 0.096 | 0.089 |
| 1000 | | 0.550 | 0.172 | 0.141 | 0.164 | 0.064 | 0.064 |
| 1100 | | 0.064 | 0.070 | 0.062 | 0.156 | 0.064 | 0.064 |

**Table 5.** Average reduction factor values of S235 10 mm steel at increasing temperatures.

| Maximum Temp. (°C) a | Test Sample Thickness (mm) | Coated | | | Uncoated | | |
|---|---|---|---|---|---|---|---|
| | | $E_a/E_a$ | $F_{a,y}/F_{a,y}$ | $F_{a,u}/F_{a,u}$ | $E_a/E_a$ | $F_{a,y}/F_{a,y}$ | $F_{a,u}/F_{a,u}$ |
| 23 | 10 | | | | 1.000 | 1.000 | 1.000 |
| 100 | | 1.000 | 1.000 | 1.000 | 1.276 | 1.120 | 1.058 |
| 200 | | 1.465 | 0.922 | 0.952 | 1.111 | 0.916 | 0.959 |
| 300 | | 0.762 | 0.793 | 0.957 | 1.277 | 0.852 | 0.907 |
| 400 | | 1.117 | 0.827 | 0.985 | 1.365 | 0.886 | 0.995 |
| 500 | | 1.021 | 0.865 | 1.000 | 1.557 | 0.749 | 0.723 |
| 600 | | 0.683 | 0.994 | 0.901 | 1.157 | 0.454 | 0.361 |
| 700 | | 0.594 | 0.732 | 0.588 | 0.663 | 0.189 | 0.140 |
| 800 | | 0.716 | 0.542 | 0.422 | 0.588 | 0.148 | 0.132 |
| 900 | | 0.356 | 0.231 | 0.170 | 0.387 | 0.084 | 0.079 |
| 1000 | | 0.444 | 0.095 | 0.088 | 0.082 | 0.067 | 0.057 |
| 1100 | | 0.277 | 0.069 | 0.061 | 0.046 | 0.039 | 0.036 |

**Table 6.** Average reduction factor values of S235 12 mm steel at increasing temperatures.

| Maximum Temp. (°C) a | Test Samples Thickness (mm) | Coated | | | Uncoated | | |
|---|---|---|---|---|---|---|---|
| | | $E_a/E_a$ | $F_{a,y}/F_{a,y}$ | $F_{a,u}/F_{a,u}$ | $E_a/E_a$ | $F_{a,y}/F_{a,y}$ | $F_{a,u}/F_{a,u}$ |
| 23 | 12 | | | | 1.000 | 1.000 | 1.000 |
| 100 | | 1.000 | 1.000 | 1.000 | 1.725 | 0.940 | 0.989 |
| 200 | | 1.175 | 1.214 | 1.112 | 1.784 | 0.738 | 0.954 |
| 300 | | 1.012 | 1.043 | 1.039 | 1.931 | 0.719 | 1.009 |
| 400 | | 0.907 | 1.226 | 1.068 | 1.414 | 0.842 | 1.045 |
| 500 | | 0.753 | 1.278 | 1.071 | 1.332 | 0.536 | 0.631 |
| 600 | | 0.557 | 1.402 | 0.939 | 1.420 | 0.442 | 0.393 |
| 700 | | 0.516 | 0.906 | 0.740 | 0.570 | 0.148 | 0.124 |
| 800 | | 0.404 | 0.530 | 0.345 | 0.841 | 0.151 | 0.142 |
| 900 | | 0.188 | 0.222 | 0.153 | 0.426 | 0.095 | 0.099 |
| 1000 | | 0.485 | 0.158 | 0.126 | 0.165 | 0.079 | 0.080 |
| 1100 | | 0.381 | 0.056 | 0.048 | 0.093 | 0.063 | 0.059 |

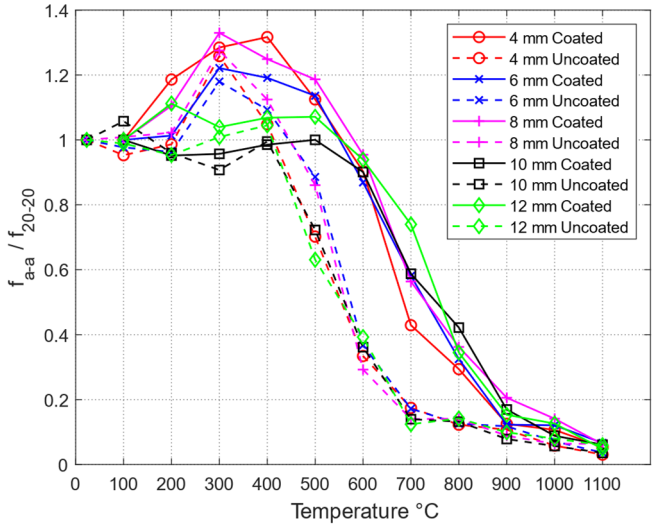


**Figure 15.** Reduction factor values of ultimate strength.

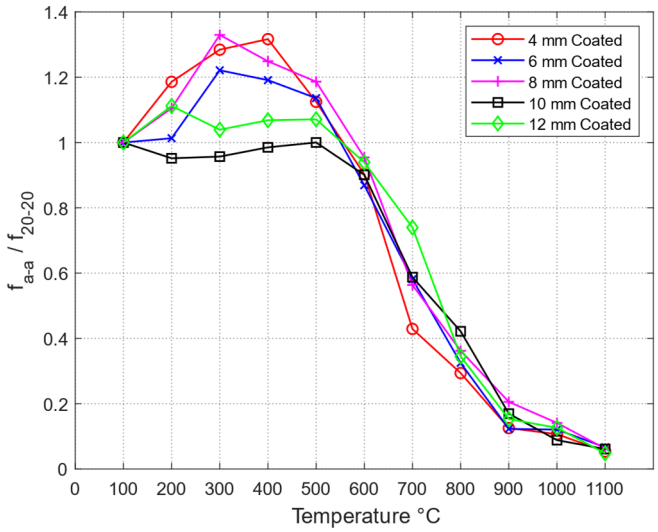


**Figure 16.** Reduction factor values of ultimate strength for coated samples.

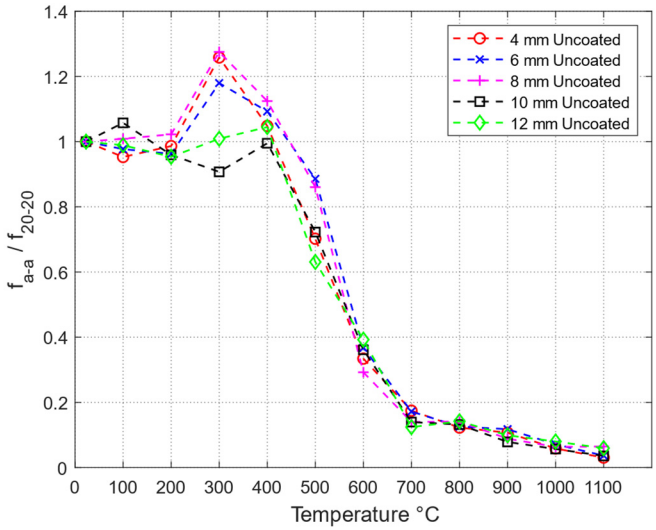


**Figure 17.** Reduction factor values of ultimate strength for uncoated samples.

The areas between coated and uncoated specimens have been calculated for each thickness. These area values represent how effectively the coat works. In other words, if the ratio of the values between coated and uncoated specimens at 500 °C is greater, the corresponding area value will be larger. Therefore, based on the magnitude of the area value, the most effective thickness for the coat's performance among the five different thicknesses will be determined. As seen in Figure 9, an area forms between coated and uncoated specimens. The area values between the reduction factors of coated and uncoated specimens are presented in Figure 6. Area values of protected/unprotected samples based on their temperature/reduction factor are given in Table 7.

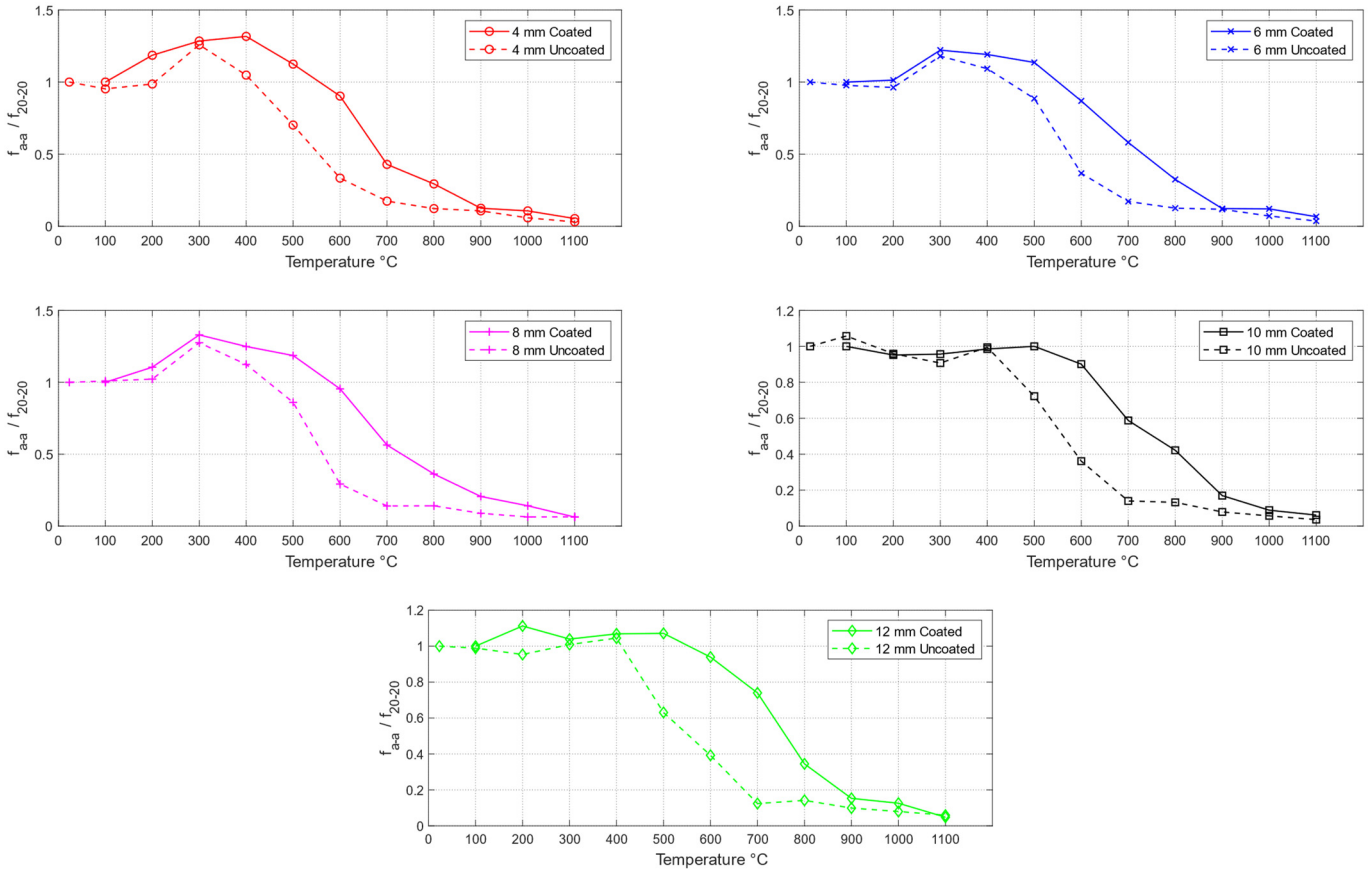


**Figure 18.** Comparison of reduction factors for fire-protected/unprotected specimens' ultimate strengths during high-temperature exposure.

**Table 7.** Area values of protected/unprotected specimens based on temperature/reduction factor.

| Wall Thickness (mm) | Area ($\frac{MPa}{MPa} * °C$) |
|---|---|
| 4 | 202 |
| 6 | 163 |
| 8 | 208 |
| 10 | 166 |
| 12 | 213 |

### *3.3. Microstructure*

The metallographic preparations of the samples used for microstructure examinations were obtained by polishing the surfaces prepared with 220–1200 grit abrasives, followed by polishing with 6-micron diamond suspensions and etching with a 5% Nital solution. The obtained surfaces were examined using the ZEN 3.5 software on the ZEISS AXIO A1 device (ZEISS, Jena, Germany).

The images obtained through optical examinations are presented in Figure 19. In microstructure examinations conducted at 700 °C, grain coarsening was observed in unpainted samples when each thickness was evaluated separately. When 700 °C painted and unpainted samples were evaluated separately, changes in the grain structure were proportional to the thickness and correlated with the tensile test results. These results, especially in the tensile test results, have emerged and led to a decrease in mechanical properties. It was determined that grain coarsening and clustering of phases occurred with the applied temperature and dwell time.

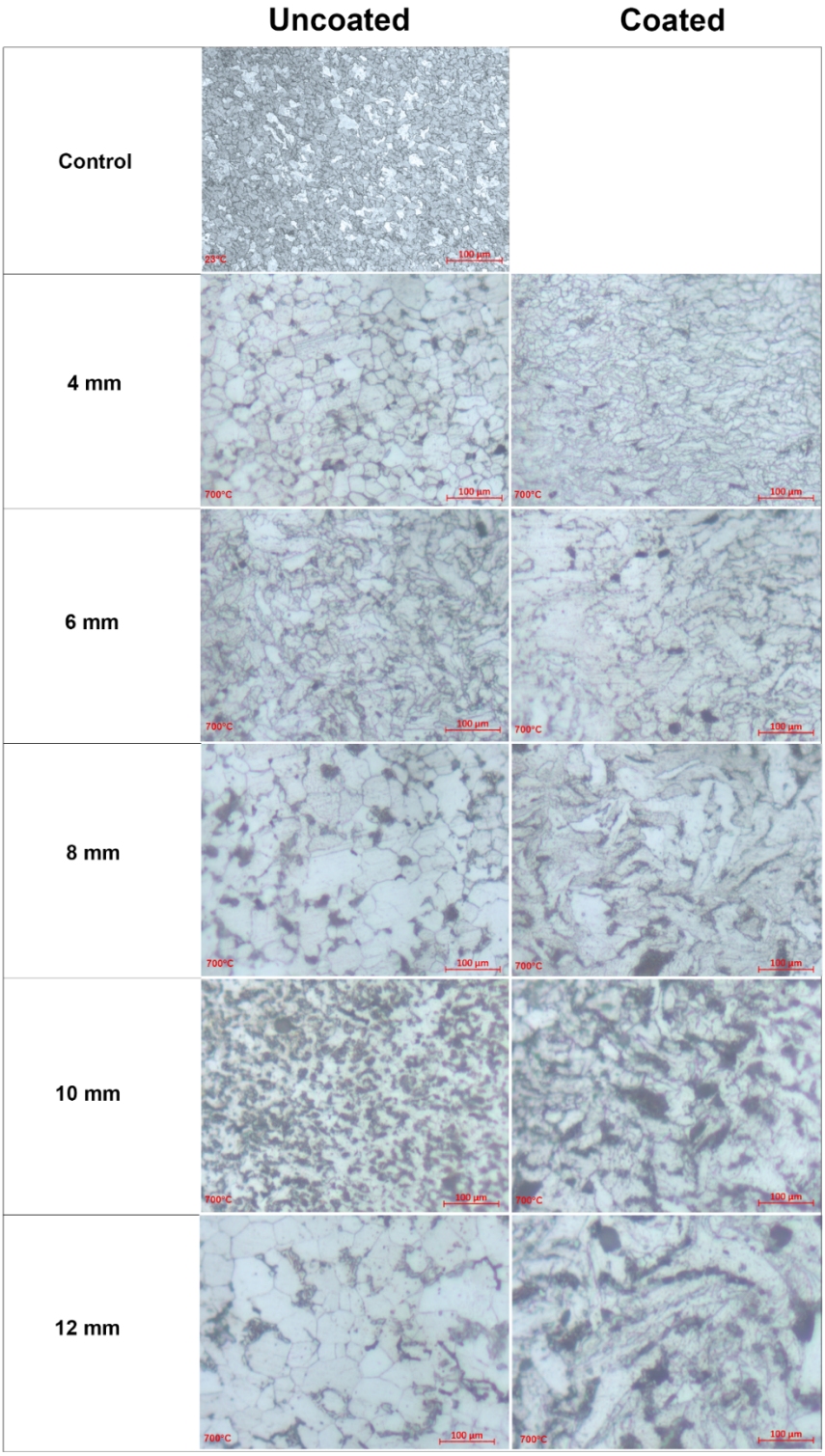


**Figure 19.** Optical microscopy images of the test specimen surfaces.

In Figure 19, the microstructural observations reveal significant changes in different samples due to temperature exposure. In particular, at 700 °C, uncoated samples show pronounced grain coarsening, indicating a deterioration in mechanical properties as a result of high-temperature exposure. This coarsening typically leads to a decrease in toughness and an increase in brittleness, adversely affecting the material's ability to withstand stress.

Comparing both painted and unpainted samples at 700 °C, the changes in grain structure correlate directly with the thickness of the specimens and the results from tensile test-

ing. Coated specimens exhibit less degradation in microstructure compared to uncoated ones, suggesting that the intumescent coating provides effective thermal protection. This protection likely helps minimize grain growth and maintain microstructural integrity more effectively than in uncoated specimens.

These microstructural changes, such as grain growth and potential phase transformations, can significantly alter the mechanical properties of steel at high temperatures. For applications involving structural steel, it is crucial to maintain a finer grain structure, as it is generally associated with higher strength and better ductility at elevated temperatures. Furthermore, the observed microstructural preservation in coated samples underscores the effectiveness of intumescent coatings. These coatings act as a barrier, reducing heat transfer to the steel substrate and thus protecting it from severe microstructural changes that compromise its structural integrity. Overall, the preservation of the microstructure in coated steel subjected to high temperatures contributes significantly to the material's mechanical performance during fire exposure. This observation warrants further analysis to fully comprehend the scope and benefits of fire-resistant coatings in maintaining the structural stability of materials in fire conditions.

### *3.4. Proposing an Analytical Model for Protected and Unprotected Specimens*

The existing experimental results were utilized to derive reduction factor (RF) equations for different thicknesses of protected and unprotected specimens under the increasing temperature effect. Analytical models were developed to predict the maximum stresses with respect to temperature, in terms of the reduction factor (RF), for specimens with thicknesses of 4, 6, 8, 10, and 12 mm in both protected and unprotected conditions. The analytical equations for protected and unprotected test specimens are provided in Table 8. Here, the RF value represents the reduction factor and T represents the temperature value. The reduction factor values obtained experimentally and those obtained from the analytical model are presented in Figure 20 for protected specimens and Figure 21 for unprotected specimens. A total of 10 analytical equations and regression coefficients are provided for the protected and unprotected specimens. Finally, analytical equations are proposed to predict the average reduction factor from the data obtained from both protected and unprotected specimens.

**Table 8.** Analytical equations predicting the reduction factor for protected/unprotected specimens.

| Specimen | Analytical Equation | Regression Coefficient R2 |
|---|---|---|
| 4 mm Coated | $RF = -3 \times 10^{-14}T^5 + 1 \times 10^{-10}T^4 - 1 \times 10^{-7}T^3 + 4 \times 10^{-5}T^2 - 0.0045T + 1.1533$ | 0.9946 |
| 6 mm Coated | $RF = -3 \times 10^{-14}T^5 + 1 \times 10^{-10}T^4 - 1 \times 10^{-7}T^3 + 5 \times 10^{-5}T^2 - 0.0085T + 1.4357$ | 0.9975 |
| 8 mm Coated | $RF = -3 \times 10^{-14}T^5 + 1 \times 10^{-10}T^4 - 1 \times 10^{-7}T^3 + 4 \times 10^{-5}T^2 - 0.0054T + 1.2143$ | 0.9955 |
| 10 mm Coated | $RF = -1 \times 10^{-14}T^5 + 5 \times 10^{-11}T^4 - 6 \times 10^{-8}T^3 + 3 \times 10^{-5}T^2 - 0.0073T + 1.4608$ | 0.994 |
| 12 mm Coated | $RF = -4 \times 10^{-15}T^5 + 2 \times 10^{-11}T^4 - 3 \times 10^{-8}T^3 + 2 \times 10^{-5}T^2 - 0.0029T + 1.1798$ | 0.9838 |
| 4 mm Uncoated | $RF = -4 \times 10^{-14}T^5 + 1 \times 10^{-10}T^4 - 1 \times 10^{-7}T^3 + 3 \times 10^{-5}T^2 - 0.0031T + 1.0374$ | 0.9768 |
| 6 mm Uncoated | $RF = -4 \times 10^{-14}T^5 + 1 \times 10^{-10}T^4 - 1 \times 10^{-7}T^3 + 4 \times 10^{-5}T^2 - 0.0049T + 1.1023$ | 0.98 |
| 8 mm Uncoated | $RF = -4 \times 10^{-14}T^5 + 1 \times 10^{-10}T^4 - 1 \times 10^{-7}T^3 + 4 \times 10^{-5}T^2 - 0.0035T + 1.0615$ | 0.9721 |
| 10 mm Uncoated | $RF = -2 \times 10^{-14}T^5 + 7 \times 10^{-11}T^4 - 6 \times 10^{-8}T^3 + 2 \times 10^{-5}T^2 - 0.0026T + 1.0796$ | 0.9782 |
| 12 mm Uncoated | $RF = -3 \times 10^{-14}T^5 + 9 \times 10^{-11}T^4 - 8 \times 10^{-8}T^3 + 3 \times 10^{-5}T^2 - 0.0032T + 1.0681$ | 0.981 |
| Average Coated | $RF = -2 \times 10^{-14}T^5 + 7 \times 10^{-11}T^4 - 8 \times 10^{-8}T^3 + 4 \times 10^{-5}T^2 - 0.0057T + 1.2888$ | 0.9978 |
| Average Uncoated | $RF = -4 \times 10^{-14}T^5 + 1 \times 10^{-10}T^4 - 1 \times 10^{-7}T^3 + 3 \times 10^{-5}T^2 - 0.0035T + 1.0698$ | 0.9842 |

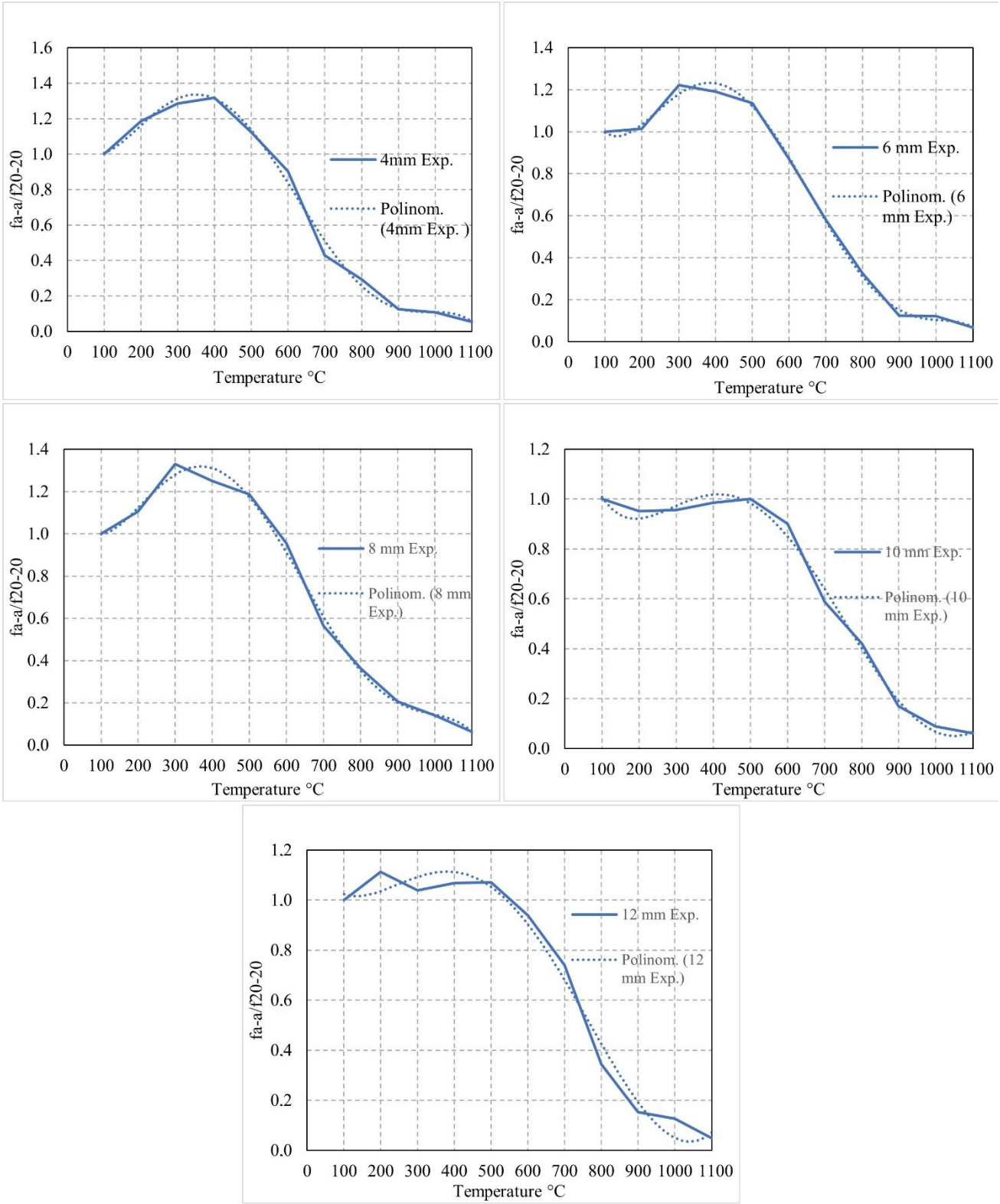


**Figure 20.** Polynomial equation predicting the reduction factor of tensile strength for coated specimens.

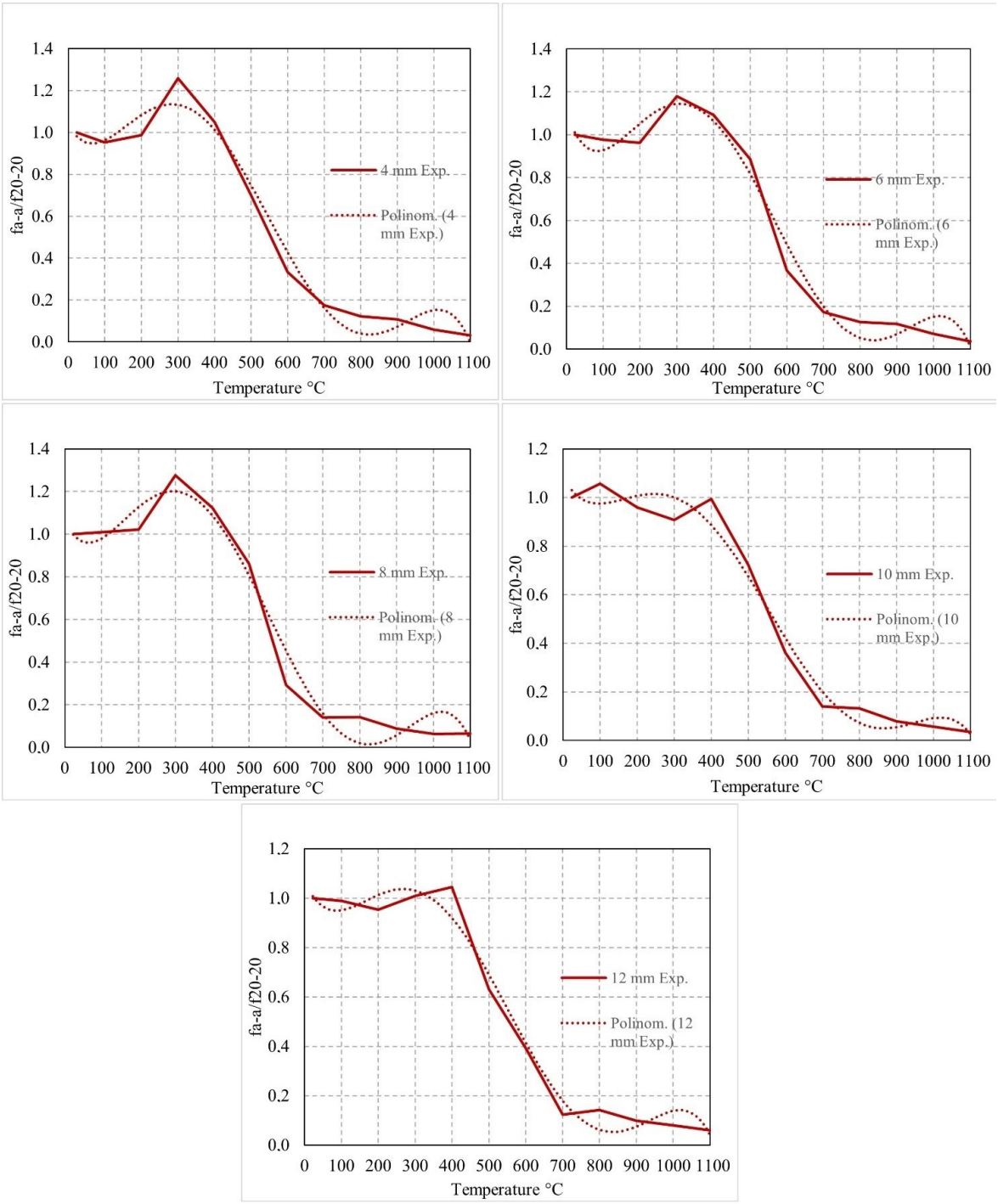


**Figure 21.** Polynomial equation predicting the reduction factor of tensile strength for uncoated specimens.

### *3.5. Comparison of the Material Properties' Decrease Factors throughout the Period of Rising Temperatures with Current Design Guidelines and Earlier Research Studies*

During the rising temperature phase in high-temperature sustained tests of S235 CFS, the ultimate strength reduction factor of S235 CFS reached its maximum value for the coatless specimens at 300 °C for thicknesses of 4, 6, and 8 mm, while specimens with thicknesses of 10 and 12 mm reached their maximum at 400 °C. For coatless specimens with thicknesses up to 8 mm, the temperature penetrated the material's internal structure, reaching the maximum value in terms of reduction factor, at 300 °C. Increases in mechanical properties were observed at up to 300 °C for thicknesses up to 8 mm. However, for speci-

mens with thicknesses of 10 and 12 mm, the maximum stress value was reached at 400 °C. After 300 °C, mechanical properties exhibited a decreasing trend. For coatless specimens with thicknesses of 10 and 12 mm, the temperature fully penetrated the material's internal structure, reaching the maximum value in terms of reduction factor at 400 °C. For specimens thicker than 8 mm, increases in mechanical properties were observed until the temperature reached 400 °C. At temperatures higher than 400 °C, there was a declining trend in mechanical properties. The temperatures at which maximum values of the reduction factor were obtained vary according to material thickness. In Figure 8, when the reduction factor values at 600 °C are carefully examined for each thickness, it can be observed that the load-bearing capacity of the section increased as the material thickness increased.

Specifically, the results indicate that the fire-protected (coated) specimens maintain a higher level of mechanical properties such as yield strength and ultimate strength at elevated temperatures up to 1100 °C. This enhanced performance is crucial in fire scenarios, as maintaining the structural integrity of steel components can be the difference between a building sustaining partial damage or succumbing to catastrophic failure. Thus, in terms of fire safety and effectiveness, our results suggest that using intumescent coatings on cold-formed steel significantly increases the material's resistance to the adverse effects of high temperatures during a fire. These findings are supported by comprehensive data showing the performance of both coated and uncoated specimens across a range of temperatures and conditions.

In this section, the reduction factor values for the maximum stresses obtained from the experimental data of S235 CFS under increasing temperature periods are compared with AS 4100 [51] and EC 3 [52] in Figure 22. In Figure 22, the reduction factor values for material property degradation during increasing temperature periods are presented. This not only reaffirms the principles laid out in the Eurocode but also provides a detailed, empirical backing for the theoretical predictions. By comparing our experimental data with the Eurocode performance criteria, we aim to bridge the gap between theoretical expectations and the real-world performance of intumescent-coated and uncoated CFS under fire conditions.

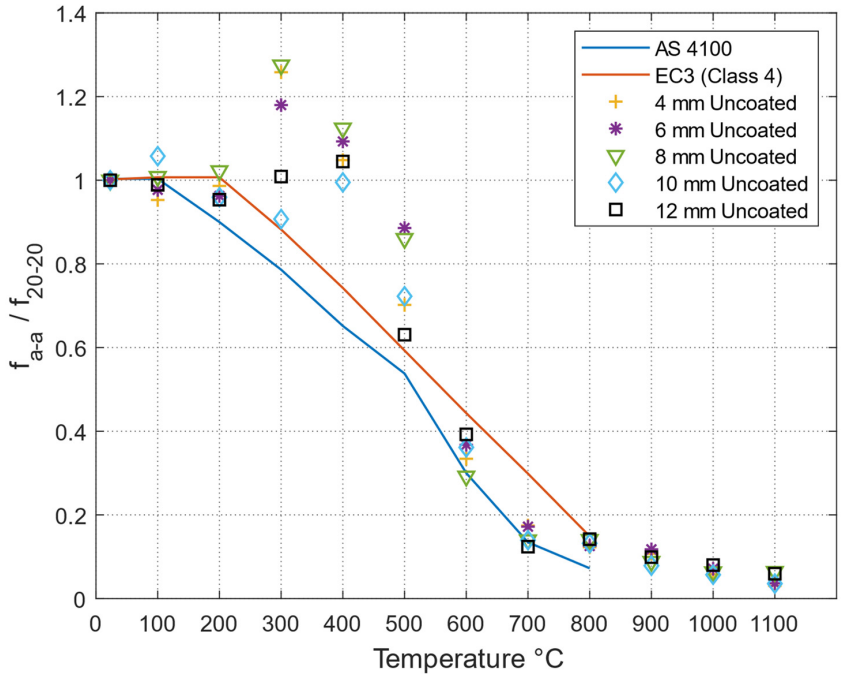


**Figure 22.** Comparison of the reduction factor values for material property degradation during the increasing temperature period with the existing design standards.

This alignment is critical for validating the Eurocode's guidelines on fire safety and for enhancing the practical understanding of fireproofing measures in structural engineering. It demonstrates that the application of intumescent coatings can effectively delay the structural degradation of CFS, thereby contributing significantly to steel structures' safety and resilience against fire.

## 4. Results

In this article, axial tensile tests were conducted on protected and unprotected conditions of S235 cold-formed steel (CFS) specimens under increasing temperature curves, where the specimens were held at the target temperature for 20 min before the initiation of the axial tensile tests. The axial carrying capacities of S235 cold-formed steel (CFS) specimens, both coated and uncoated, have been observed to increase with the thickness of the steel across various temperature exposures up to 300–400 °C. This trend underscores the importance of material thickness in maintaining structural integrity under high-temperature conditions. The performance of coated specimens is particularly notable, as they consistently exhibited higher strength values compared to their uncoated counterparts, especially within the critical temperature range of 500–900 °C. The efficacy of intumescent coatings in reducing the temperature exposure of steel by approximately 200 °C plays a crucial role in preserving the mechanical properties during fire exposure. The following results have been obtained:

(1) During the increasing temperature periods, the material properties of S235 CFS exhibit an increase in mechanical characteristics as the test temperature rises, dependent on the material thickness. However, it is important to note that variations in test results according to the thickness of the material are considerable during the increasing temperature cycles. In general, under the same temperatures, as the thickness of the material increases during the rising temperature period, mechanical properties tend to be slightly higher or in close proximity to each other. The standard deviation of the reduction factors in ultimate strength among the increasing temperature cycles ranges from 0% to 16.09% for coated specimens and from 0.9% to 16.14% for uncoated specimens. Therefore, from an engineering design perspective, when using reduction factor values in terms of ultimate strength for coated and uncoated specimens based on material thicknesses during the rising temperature periods, the calculation results for fire-induced deformation in S235 CFS elements can be more reliable.

(2) When examining uncoated specimens separately, for specimen thicknesses up to 8 mm, an increase in mechanical properties was observed at temperatures of up to 300 °C, while for specimens thicker than 8 mm, mechanical properties reached their maximum at 400 °C. However, after these specified temperatures, there is a general decreasing trend up to 700 °C. Between 700 °C and 1100 °C, the trend of decrease is less steep.

(3) When examining coated specimens separately, for specimen thicknesses up to 8 mm, there was an increase in mechanical properties in the range of 300–400 °C. For specimens thicker than 8 mm, mechanical properties did not show significant variation up to 500 °C. Between 500 °C and 900 °C, there was a general decreasing trend. Between 900 °C and 1100 °C, the trend of decrease was less steep.

(4) Between 500 °C and 1100 °C, the mechanical properties of coated specimens were significantly higher than those of uncoated specimens. The ratio of the reduction factors of ultimate stresses for coated specimens to the reduction factors of ultimate stresses for uncoated specimens reached 5.96. This value holds significant importance for the fire resistance of steel structural systems. In real fire situations, the structural system must bear both the load and the effects of the fire. Therefore, the scenario of fire exposure combined with structural loading has been considered. The primary behavior of fire-retardant coats is observed when both fire exposure and structural loading are combined. These combined conditions have identified significant differences in the mechanical properties of coated and uncoated specimens.

(5) When comparing coated and uncoated specimens within each thickness, it was observed that the coat was most effective in the 12 mm thickness samples. In other words, the performance of the coat varies according to the thickness of the specimen. Additionally, it is anticipated that changes in performance values will also occur as the coat thickness is altered.

(6) Coated specimens consistently demonstrated higher strength values than their uncoated counterparts, particularly at temperatures ranging from 500 to 900 °C. This suggests that the coatings not only protect against thermal degradation but also contribute significantly to maintaining structural integrity under fire conditions. Notably, the onset of significant degradation in mechanical properties was observed at higher temperatures for coated specimens compared to uncoated ones, with coated specimens beginning to show strength losses at temperatures beyond 500 °C, compared to 400 °C for uncoated specimens.

(7) Across all tested thicknesses, coated specimens generally exhibited higher ultimate strength values, especially as temperatures approached critical levels. This enhanced performance underscores the coatings' effectiveness in scenarios where steel structures are exposed to high temperatures for extended periods.

(8) Furthermore, the impact of specimen thickness was pronounced. Both coated and uncoated specimens showed increased ultimate strength, with greater material thickness at temperatures up to 300–400 °C. However, this benefit was more noticeable in coated specimens, indicating that the effectiveness of intumescent coatings is augmented in thicker sections of steel.

**Funding:** This research received no external funding.

**Data Availability Statement:** The original contributions presented in the study are included in the article, further inquiries can be directed to the corresponding authors.

**Conflicts of Interest:** The authors declare no conflict of interest.

## References

1. Yu, Y.; Lan, L.; Ding, F.; Wang, L. Mechanical properties of hot-rolled and cold-formed steels after exposure to elevated temperature: A review. *Constr. Build. Mater.* **2019**, *213*, 360–376. [CrossRef]
2. McCann, F.; Gardner, L.; Kirk, S. Elevated temperature material properties of cold-formed steel hollow sections. *Thin-Walled Struct.* **2015**, *90*, 84–94. [CrossRef]
3. Choi, I.-R.; Chung, K.-S.; Kim, D.-H. Thermal and mechanical properties of high-strength structural steel HSA800 at elevated temperatures. *Mater. Des.* **2014**, *63*, 544–551. [CrossRef]
4. Rokilan, M.; Mahendran, M. Elevated temperature mechanical properties of cold-rolled steel sheets and cold-formed steel sections. *J. Constr. Steel Res.* **2020**, *167*, 105851. [CrossRef]
5. Pieper, L.; Mahendran, M. Mechanical properties of cold-formed steel cladding profiles at elevated temperatures. *Thin-Walled Struct.* **2021**, *164*, 107773. [CrossRef]
6. Imran, M.; Mahendran, M.; Keerthan. Mechanical properties of cold-formed steel tubular sections at elevated temperatures. *J. Constr. Steel Res.* **2018**, *143*, 131–147. [CrossRef]
7. Ban, H.; Zhou, G.; Yu, H.; Shi, Y.; Liu, K. Mechanical properties and modelling of superior high-performance steel at elevated temperatures. *J. Constr. Steel Res.* **2021**, *176*, 106407. [CrossRef]
8. Yazici, C.; Özkal, F.M.; Orhan, S.N.; Cirpici, B.K. Reformative Effects of Intumescent Coating on the Structural Characteristics of Cold-Formed Steel. *ACS Omega* **2022**, *7*, 42560–42569. [CrossRef] [PubMed]
9. Cirpici, B.K.; Orhan, S.N.; Yazici, C.; Özkal, F.M. Numerical Investigation of the Fire Behavior of Storage Rack Systems Protected by Intumescent Coating. *ACS Omega* **2022**, *7*, 36001–36008. [CrossRef]
10. *EN 1993-1-2*; Eurocode 3: Design of Steel Structures—Part 1-2: General Rules—Structural Fire Design. British Standards Institution: London, UK, 2005.
11. Chen, W.; Ye, J.; Bai, Y.; Zhao, X.L. Full-scale fire experiments on load-bearing cold-formed steel walls lined with different panels. *J. Constr. Steel Res.* **2012**, *79*, 242–254. [CrossRef]
12. Chen, W.; Ye, J.; Bai, Y.; Zhao, X.L. Improved fire resistant performance of load bearing cold-formed steel interior and exterior wall systems. *Thin-Walled Struct.* **2013**, *73*, 145–157. [CrossRef]
13. Feng, M.; Wang, Y.C. An experimental study of loaded full-scale cold-formed thin-walled steel structural panels under fire conditions. *Fire Saf. J.* **2005**, *40*, 43–63. [CrossRef]

14. Ariyanayagam, A.D.; Mahendran, M. Experimental study of non-load bearing light gauge steel framed walls in fire. *J. Constr. Steel Res.* **2018**, *145*, 529–551. [CrossRef]
15. Li, H.T.; Young, B. Cold-formed high strength steel SHS and RHS beams at elevated temperatures. *J. Constr. Steel Res.* **2019**, *158*, 475–485. [CrossRef]
16. Cirpici, B.K. Design analysis of a steel industrial building with wide openings exposed to fire. *Chall. J. Struct. Mech.* **2020**, *6*, 99. [CrossRef]
17. Çırpıcı, B.K.; Orhan, S.N.; Kotan, T. Numerical modelling of heat transfer through protected composite structural members. *Chall. J. Struct. Mech.* **2019**, *5*, 96. [CrossRef]
18. Cirpici, B.K.; Orhan, S.N.; Kotan, T. Finite element study on composite slab-beam systems under various fire exposures. *Steel Compos. Struct.* **2020**, *37*, 589–603. [CrossRef]
19. Cirpici, B.K.; Wang, Y.C.; Rogers, B. Assessment of the thermal conductivity of intumescent coatings in fire. *Fire Saf. J.* **2016**, *81*, 74–84. [CrossRef]
20. Cirpici, B.K.; Wang, Y.C.; Rogers, B.; Bourbigot, S. A Theoretical Model for Quantifying Expansion of Intumescent Coating Under Different Heating Conditions. *Polym. Eng. Sci.* **2016**, *56*, 798–809. [CrossRef]
21. Chen, W.; Ye, J.; Jin, L.; Jiang, J.; Liu, K.; Zhang, M.; Chen, W.; Zhang, H. High-temperature material degradation of Q345 cold-formed steel during full-range compartment fires. *J. Constr. Steel Res.* **2020**, *175*, 106366. [CrossRef]
22. Yazici, C.; Arik, E.; Özkal, F.M. Influence of design parameters on beam-to-column connections of steel storage rack systems. *Eng. Fail. Anal.* **2023**, *152*, 107439. [CrossRef]
23. Kang, S.; Choi, J.Y.; Choi, S. Mechanism of heat transfer through porous media of inorganic intumescent coating in cone calorimeter testing. *Polymers* **2019**, *11*, 221. [CrossRef] [PubMed]
24. *EN 15512*; Steel Static Storage Systems—Adjustable Pallet Racking Systems—Principles for Structural Design. British Stand-ards Institution: London, UK, 2009.
25. Came, C. Steel Buildings in Europe Multi-Storey Steel Buildings Part 6: Fire Engineering. Available online: https://www.steelconstruction.info/images/c/c1/SBE_MS6.pdf (accessed on 24 March 2024).
26. Bilotta, A.; De Silva, D.; Nigro, E. STRUCTURAL FIRE SAFETY OF EXISTING STEEL BUILDINGS, Possible general approach and application to the case of the intumescent coatings. *Appl. Struct. Fire Eng.* **2015**, 15–16. [CrossRef]
27. Bilotta, A.; de Silva, D.; Nigro, E. Tests on intumescent paints for fire protection of existing steel structures. *Constr. Build. Mater.* **2016**, *121*, 410–422. [CrossRef]
28. Jimenez, M.; Duquesne, S.; Bourbigot, S. Intumescent fire protective coating: Toward a better understanding of their mecha-nism of action. *Thermochim. Acta* **2006**, *449*, 16–26. [CrossRef]
29. Bugajny, M.; Le Bras, M.; Bourbigot, S. New approach to the dynamic properties of an intumescent material. *Fire Mater.* **1999**, *23*, 49–51. [CrossRef]
30. Gardelle, B.; Duquesne, S.; Rerat, V.; Bourbigot, S. Thermal degradation and fire performance of intumescent silicone-based coatings. *Polym. Adv. Technol.* **2013**, *24*, 62–69. [CrossRef]
31. Lucherini, A.; Maluk, C. Intumescent coatings used for the fire-safe design of steel structures: A review. *J. Constr. Steel Res.* **2019**, *162*, 105712. [CrossRef]
32. Mariappan, T. Recent developments of intumescent fire protection coatings for structural steel: A review. *J. Fire Sci.* **2016**, *34*, 120–163. [CrossRef]
33. Wang, Y.C.; Bailey, C.G. *Temperature Distribution in Intumescent Coating Protected Steel Connections in Fire*; School of Mechanical, Aerospace and Civil Engineering: Manchester, UK, 2017.
34. Wang, W.; Liu, T.; Liu, J. Experimental study on post- fire mechanical properties of high strength Q460 steel. *J. Constr. Steel Res.* **2015**, *114*, 100–109. [CrossRef]
35. Yuan, J.F.; Wang, Y.C. Chapter 15: Efficient Modelling of Temperatures in Steel Plates Protected by Intumescent Coating in Fire. In *Fire Retardancy of Polymers*; Woodhead Publishing: Cambridge, UK, 2009; pp. 225–239. [CrossRef]
36. Zhang, Y.; Wang, Y.C.; Bailey, C.G.; Taylor, A. Global modelling of fire protection performance of intumescent coating under different cone calorimeter heating conditions. *Fire Saf. J.* **2012**, *50*, 51–62. [CrossRef]
37. Zhang, Y.; Wang, Y.C.; Bailey, C.G.; Taylor, A. Global modelling of fire protection performance of an intumescent coating under different furnace fire conditions. *J. Fire Sci.* **2013**, *31*, 51–72. [CrossRef]
38. Horacek, H. Reactions of Stoichiometric Intumescent Paints. *J. Appl. Polym. Sci.* **2008**, *116*, 2658–2667. [CrossRef]
39. Weisheim, W.; Schaumann, P.; Sander, L.; Zehfuß, J. Numerical model for the fire protection performance and the design of intumescent coatings on structural steel exposed to natural fires. *J. Struct. Fire Eng.* **2020**, *11*, 33–50. [CrossRef]
40. Schaumann, P.; Kirsch, T. Protected steel and composite connections: Simulation of the mechanical behaviour of steel and composite connections protected by intumescent coating in fire. *J. Struct. Fire Eng.* **2015**, *6*, 41–48. [CrossRef]
41. Kraus, P.; Mensinger, M.; Tabeling, F.; Schaumann, P. Experimental and numerical investigations of steel profiles with intumescent coating adjacent to space-enclosing elements in fire. *J. Struct. Fire Eng.* **2015**, *6*, 237–246. [CrossRef]
42. Ren, C.; Zhang, P.; Yan, S.; Dai, L. Analysis and design of cold-formed steel storage rack uprights under localised fires. *Structures* **2020**, *27*, 2082–2095. [CrossRef]
43. Chen, W.; Liu, K.; Ye, J.; Jin, L. Influence of test parameters on the high-temperature material properties of G550 CFS. *J. Constr. Steel Res.* **2022**, *197*, 107478. [CrossRef]

44. Beh, J.H.; Yew, M.C.; Yew, M.K.; Saw, L.H. Fire Protection Performance and Thermal Behavior of Thin Film Intumescent Coating. *Coatings* **2019**, *9*, 483. [CrossRef]
45. *BS 476*; Fire tests on Building Materials and Structures—Part 6: Method of Test for Fire Propagation for Products. British Standards Institution: London, UK, 1989.
46. Zhang, Q.; Wang, Q.; Li, Y.; Li, Z.; Liu, S. Effects and Mechanisms of Ultralow Concentrations of Different Types of Graphene Oxide Flakes on Fire Resistance of Water-Based Intumescent Coatings. *Coatings* **2024**, *14*, 162. [CrossRef]
47. Riva, M.; Costa, E.; Massabò, V.; Gaggero, M.; Lacidogna, C. Damage Investigation of Intumescent Coating under Different Environmental Conditions by Acoustic Emission and Artificial Neural Networks. *Coatings* **2020**, *10*, 1117.
48. Soudani, M.; Brosseau, J.; Ahmed, E.; Kaddami, S. Waterborne Silica/Epoxy Intumescent Coatings: Towards Fire Retardant Nanocomposite Coatings. *Polymers* **2020**, *12*, 757.
49. Xie, C.; Jiang, Z.; Wang, Q.; Yu, J.; Tang, Y. Enhanced Fire Resistance and Mechanical Properties of Intumescent Fire Retardant Coating with Incorporation of Halloysite Nanotubes. *Polymers* **2021**, *13*, 2620.
50. Kiziltas, H.; Biris, A.A.; Uzun, S.; Eckert, G.M. Thermal; Mechanical, and Ablative Properties of Intumescent Flame-Retardant Coatings Using Multiwall Carbon Nanotubes. *Coatings* **2023**, *13*, 495.
51. *ISO 10138:1991*; Steel and Cast Iron—Determination of Chromium Content—Diphenylcarbazide Spectrophotometric Method. ISO: Geneva, Switzerland, 1984.
52. Code, P. *Eurocode 3: Design of Steel Structures-Part 1–2: General Rules-Structural Fire Design*; European Committee for Standardisation: London, UK, 2007.